COMMISSIONING STATUS OF THE ASTA FACILITY AT FERMILAB*

A.H. Lumpkin#, J. Ruan, D. Broemmelsiek, D. Crawford, D. Edstrom, N. Eddy, E. Harms, J. Hocker, J. Leibfritz, J. Santucci, G. Stancari, D. Sun, J. Thangaraj, R. Thurman-Keup, A. Warner, and J. Zhu
Fermi National Accelerator Laboratory, Batavia, IL 60510 USA

Abstract

Early commissioning results and status of the Advanced Superconducting Test Accelerator (ASTA) at Fermilab will be described. The ASTA facility will consist of an L-band rf photocathode (PC) gun, two superconducting L-band rf booster cavities, transport lines, and an 8-cavity TESLA style cryomodule. Early results include first photoelectrons from the Cs_2Te photocathode and operations at 3-5 MeV from the rf PC gun. Measurements of beam size, position, energy, and charge have been obtained with the beam profile station and Faraday cup at that low energy location. Diagnostics for the 20-50 MeV energy beam are also described as well as the first conditioning results for the cryomodule cavities.

INTRODUCTION

The Advanced Superconducting Test Accelerator (ASTA) facility [1] is currently being constructed at Fermilab with initial commissioning steps already in progress. The electron beam has been generated in a photoinjector based on a UV drive laser and the L-band rf photocathode (PC) gun cavity which is shown in Fig. 1. Low energy results at 3-5 MeV sampled after the gun are described. Initial commissioning of beam to the low energy beam dump will be done with one booster cavity. The beam line with one 4-dipole chicane, extensive diagnostics, and spectrometer has been installed in the linac for 20-50 MeV operations in the coming months. Downstream of this location is the 8-cavity cryomodule in which all cavities have been operated individually. Updated cryomodule results will be presented. The feasibility of using the commissioned linac and cryomodule to provide 300-MeV beams to drive EUV FEL oscillator tests at 120 nm was described previously [2].

EXPERIMENTAL ASPECTS

The injector portion of the facility, the first cryomodule, and the proposed FEL oscillator configuration are shown in Fig. 2. After the L-band rf pC gun, two L-band superconducting booster cavities will provide up to 50 MeV acceleration capability. At this time, the first cavity has been temporarily replaced by a spool piece, and the second cavity has been installed and conditioned to 20 MV/m. Only results from the diagnostics after the rf gun and cryomodule conditioning will be presented.

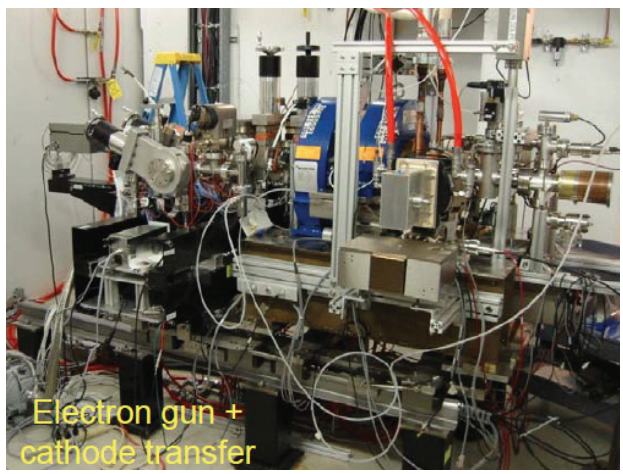

Figure 1: The L-band photoinjector with photocathode transfer hardware, and with two solenoid magnets.

The Drive Laser

The drive laser is based on an Yb fiber laser oscillator running at 1.3 GHz that is then divided down to 81.25 MHz and amplified. The four-stage origination and amplification is a set of commercial components from Calmar collectively referred to as the seed laser in the context of ASTA. The 81.25 MHz packets of IR laser, at a wavelength of 1053 nm is directed into a multi-pass amplifier (MPA), which provides amplified pulses at a 3 MHz rate that are then pulse cleaned with two sets of Pockels cells. The MPA has recently been replaced by a preamp composed of three single pass stages. A third Pockels cell, referred to as the pulse picker is not currently being used. Three YLF-based single-pass amplifiers (SPA) and a Northrup-Grumman SPA (NGA) boost the energy to several μJ per pulse before the two doubling crystal stages that generate the green and then the UV components at 3 MHz [3]. The UV is transported out of the laser lab through the UV transport line to the photocathode of the gun for generation of the photoelectron beams for the SC rf accelerator [1].

Base Electron Beam Diagnostics

The base beam profile imaging stations have been equipped with both YAG:Ce scintillators and optical transition radiation (OTR) screens, optical transport, and digital CCD cameras. The Gig-E vision protocol has been supported by selection of the Prosilica 5 Mpix cameras for

*Work supported under Contract No. DE-AC02-07CH11359 with the United States Department of Energy.
#lumpkin@fnal.gov

ISBN 978-3-95450-133-5

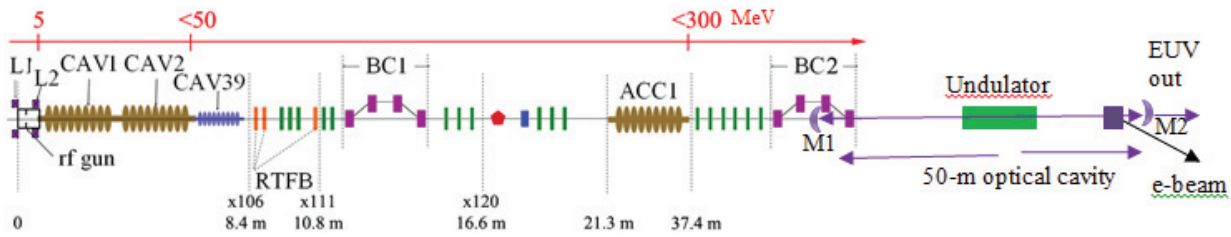

Figure 2: Schematic of the ASTA linac showing the rf gun, solenoids L1 and L2, the L-band booster cavities (CAV1 and CAV2), a proposed third harmonic linearizing cavity, chicane BC1, the first cryomodule (ACC1), and the proposed FEL oscillator configuration.

the beamline profiling stations and the 1.3 Mpixel camera with 2/3" format for the streak cameras. We have then used both the online Java-based ImageTool and the offline MATLAB-based ImageTool processing programs [4,5] in the commissioning of the system. The commissioning of the UV drive laser and the comprehensive measurements with the streak camera are described elsewhere in this conference [6]. A set of rf BPMs, wall current monitors, and toroids are also being implemented.

The Hamamatsu Streak Camera Systems

Commissioning of the laser lab streak camera system was facilitated through a new suite of controls centered around ACNET, the Fermilab accelerator controls network. This suite included operational drivers to control and monitor the streak camera, as well as Java-based programs to interface with the driver and retrieve images from the readout camera. This commissioning period allowed a number of improvements to be made to all aspects of interfacing with the C5680 streak camera, both in terms of software and hardware [6].

For the electron beam studies, the second streak camera is also a Hamamatsu C5680 mainframe with S20 PC streak tube and can accommodate a vertical sweep plugin unit and a horizontal sweep unit or blanking unit. The all-mirror input optics enables the assessment of the UV OTR component as well as the visible light OTR. These optics also mitigate the streak image blurring due to the inherent chromatic temporal dispersive effects of the lens-based input optics for broadband sources such as OTR. The studies will start with the M5675 synchroscan unit with its resonant circuit tuned at 81.25 MHz so the streak image would have jitter of less than 1 ps from the system itself.

Bunch Length Monitor at 20-50 MeV

We have developed plans for the bunch length monitor station that will be located after the chicane at X121 as shown in Fig. 3. An Al-coated Si wafer rotated at 45 degrees to the beam direction will serve as the converter screen (36 mm x 25 mm) for generation of coherent transition radiation (CTR), coherent diffraction radiation (CDR), and incoherent OTR. The three sources are schematically shown in Fig. 4. Initially, the lower screen edge will be moved above the beam center to allow the nonintercepting generation of CDR instead of using an aperture in a screen. The THz signals will be detected by pyroelectric detectors, and the MPI will be employed for bunch length evaluation. The OTR will be transported in an enclosed pipe outside of the tunnel to the streak camera station.

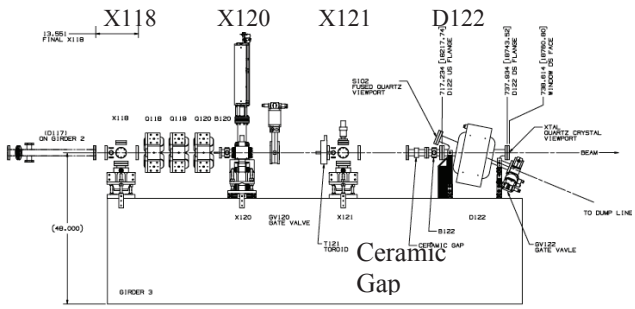

Figure 3: Post-chicane area (Girder 3) with quads and planned imaging stations X118, X120, and X121 and the ceramic gap.

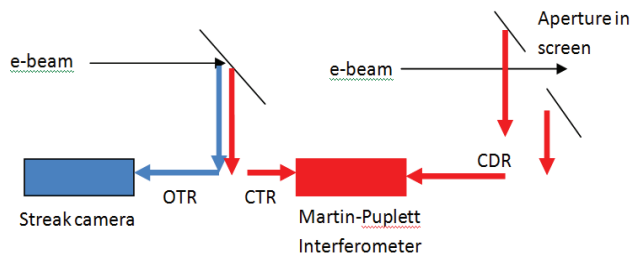

Figure 4: Schematic of a three-source option for OTR, CTR, and CDR diagnostics with the streak camera and MPI indicated. The OTR/CTR screen is at the left, and the CDR screen with aperture is at the right.

In addition a ceramic gap monitor located downstream of the X121 station as indicated in Fig. 3 will be used to assess bunch length. The expected temporal resolutions for the techniques are provided in Table 1 as compared to alternative rf deflector techniques. The rf deflector installations have been postponed. The streak camera viewing OTR and MPI via CTR will be used to evaluate the ceramic gap monitor performance with low power beam at the 1 ps level. With high power beam we will adjust the Al screen lower edge to be a few mm above the beam line center and use the CDR with MPI to compare to the ceramic gap results.

ISBN 978-3-95450-133-5

Table 1: Summary of Bunch Length Monitor Options with Technique, Resolution, and Estimated Charge Needed

Technique	Resolution	Charge needed
Streak camera	~0.6 ps sigma at 800 nm, range 0.5-25ps, phase stable*	8-10 nC
MPI	0.3 ps, range 0.3 to 1ps. CTR,CSR,CDR	10-50 nC, depends on σ_t
Ceramic gap	0.5 to 5ps	TBD
RF cavity, L-band	0.5 ps estimated	250 pC with scintillator screen
RF cavity, 3.9 GHz	TBD	250 pC with scintillator screen

EXPERIMENTAL RESULTS

Initial PC RF Gun Results

The rf PC gun studies were initiated last year on June 20, 2013 by using just the Mo substrate as a low quantum efficiency cathode. With a few uJ of energy per UV pulse, we generated a few pC per micropulse. Since that time the Cs_2Te coated cathodes with about 1 to 1.5 % Q.E. were installed in the transfer chamber, and one subsequently inserted into rf gun back plane. Micropulse charges of 20 to 1000 pC were generated for 100 µs at 3 MHz. One of the first images is shown in Fig. 5, and an early evaluation of beam energy versus the gun rf power is shown in Fig. 6. The plots show both data extracted from the solenoid field scan and the use of the corrector magnets to cause measurable beam deflections. The highest power gave a gradient of about 45 MV/m. A few runs were done with 3000 micropulses to exercise the laser system at the design macropulse length, but with reduced charge per micropulse as seen in Fig. 7. This kind of macropulse when accelerated by the linac and cryomodule and bunch compressed could support an FEL oscillator configuration at 120 nm. The schematic of this implementation is shown in Fig. 2, and the simulations are given in reference [2].

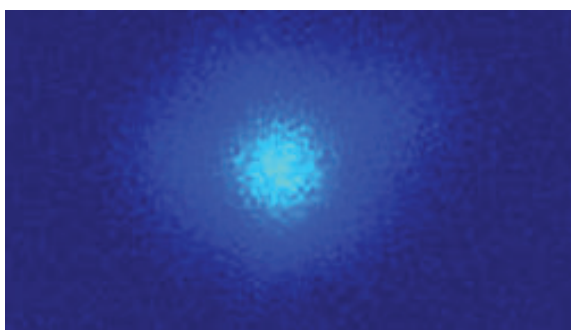

Figure 5: Image of beam at 4 MeV from the gun using the YAG:Ce converter screen and digital CCD camera. It was sub-mm (sigma) beam size [7].

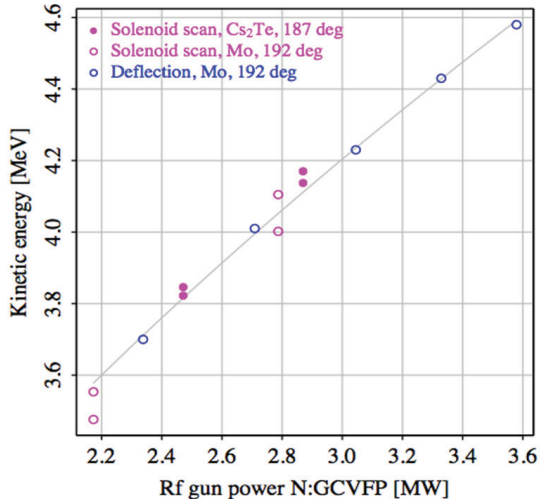

Figure 6: Electron beam energy after the gun vs. rf gun power [8].

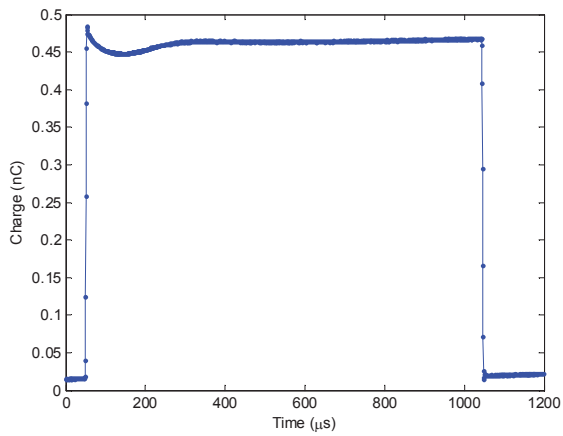

Figure 7: Demonstration of 1-ms-long macropulse of photoelectrons with about 0.45 nC per micropulse as measured at the low energy Faraday cup [8].

Cryomodule Cavity Conditioning Results

The eight cavities in the cryomodule presently installed in the tunnel as shown in Fig. 8 have been rf conditioned individually. All but one reached the targeted 31.5 MV/m gradient as shown in the plots of Fig. 9 [9]. The one reached 30.5 MV/m. The average of the eight cavity gradients is still 31.3 MV/m, which is the highest value demonstrated in a cryomodule to date. The plots of the cavity gradients in the vertical and horizontal test stands are also shown for comparison in Fig. 9. Details were presented at IPAC14 [9]. More recently cavities 1-7 have been powered at the same time through an rf power distribution system and attained > 30 MV/m average in initial conditioning tests.

ISBN 978-3-95450-133-5

Figure 8: Cryomodule as installed in the ASTA tunnel before the waveguide distribution system was installed.

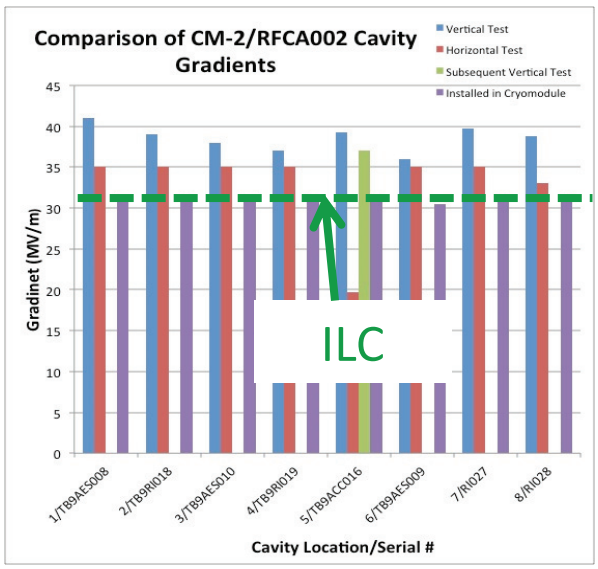

Figure 9: Plot of the cavity gradients attained in the vertical test stand (blue), horizontal test stand (red), and when installed in the CM-2 cryomodule (purple). The 31.5 MV/m value was a target and initial administrative limit in the cryomodule tests [9].

SUMMARY

In summary, we have described a series of commissioning results on first beam from the gun and first tests at high gradient of the SCRF cavities in the cryomodule. We are poised to accelerate beam to 20+ MeV and to begin full characterization of the beam properties. Eventually we will extend the beamline to the high energy beam dump and then inject beam into the cryomodule to evaluate higher order modes under beam loading conditions.

ACKNOWLEDGMENTS

The authors acknowledge the generation of ACNET controls for the various systems by C. Briegel; the development of the Java-based ImageTool code by J. Diamond, the 81.25 MHz rf source provided by B. Chase, and efforts of the mechanical support and clean room personnel of Fermilab's Accelerator and Technical Divisions.

REFERENCES

[1] The ASTA User Facility Proposal, Fermilab-TM-2568, October 2013.

[2] A.H. Lumpkin et al., "Feasibility of an XUV FEL Oscillator at ASTA", in *Proc. 35th Int. Free-Electron Laser Conf.*, New York, 2013, pp. 88-91.

[3] J. Ruan, M. Church, D. Edstrom, T. Johnson, and J. Santucci, in *Proc. of Int. Particle Accel. Conf.*, Shanghai, 2013, WEPME057.

[4] J. Diamond, FNAL, online Java-based ImageTool, (2013).

[5] R.Thurman-Keup, FNAL, offline MATLAB-based ImageTool (2011).

[6] A.H. Lumpkin, C. Edstrom, J. Ruan, and J. Santucci, "Commissioning of a Dual-Sweep Streak Camera with Applications to the ASTA Photoinjector Drive Laser", in *These Proceedings: Proc. 36th Int. Free-Electron Laser Conf.*, Basel, 2014, MOP021.

[7] D. Crawford et al., "Assembly and Installation of Beam Instrumentation for the ASTA Front-end Diagnostic Table", in *Proc. of the Int. Particle Accel. Conf.*, Dresden, 2014, pp.3732-3734.

[8] J. Ruan et al., "Commissioning Status of the Advanced Superconducting Accelerator at Fermilab", in *Proc. of the Int. Particle Accel. Conf.*, Dresden, 2014, WEPRI058.

[9] E. Harms et al., "SRF Systems for ASTA at Fermilab", in *Proc. of the Int. Particle Accel. Conf.*, Dresden, 2014, WEPRI052.

ISBN 978-3-95450-133-5